Perspectives and limitations of QKD integration in metropolitan area networks

Authors: Slavisa Aleksic, Florian Hipp, Dominic Winkler, Andreas Poppe, Bernhard Schrenk, and Gerald Franzl

Perspectives and limitations of QKD integration in metropolitan area networks

Slavisa Aleksic,[1] * **Florian Hipp,**[2] **Dominic Winkler,**[1] **Andreas Poppe,**[2] **Bernhard Schrenk,**[2] **and Gerald Franzl**[1]

[1] *Vienna University of Technology, Institute of Telecommunications, Favoritenstr. 9-11/E389, Vienna, Austria*

[2] *Digital Safety & Security Department, Optical Quantum Technology, AIT Austrian Institute of Technology GmbH, Donau-City-Strae 1, 1220 Vienna, Austria*

* *slavisa.aleksic@tuwien.ac.at.*

Abstract: Quantum key distribution (QKD) systems have already reached a reasonable level of maturity. However, a smooth integration and a wide adoption of commercial QKD systems in metropolitan area networks has still remained challenging because of technical and economical obstacles. Mainly the need for dedicated fibers and the strong dependence of the secret key rate on both loss budget and background noise in the quantum channel hinder a practical, flexible and robust implementation of QKD in current and next-generation optical metro networks.

In this paper, we discuss these obstacles and present approaches to share existing fiber infrastructures among quantum and classical channels. Particularly, a proposal for a smooth integration of QKD in optical metro networks, which implies removing spurious background photons caused by optical transmitters, amplifiers and nonlinear effects in fibers, is presented and discussed. We determine and characterize impairments on quantum channels caused by many classical telecom channels at practically used power levels coexisting within the same fiber. Extensive experimental results are presented and indicate that a practical integration of QKD in conventional optical metro networks is possible.

OCIS codes: (060.4510) Optical communications; (060.5565) Quantum communications; (270.5568) Quantum cryptography.

References and links

1. C. Bennett and G. Brassard, "Quantum cryptography: public key distribution and coin tossing," IEEE Intern. Conf. on Comp. Syst. and Sign. Process., Bangalore, IEEE, 1291–1293 (1984).
2. L. Lydersen, C. Wiechers, C. Wittmann, D. Elser, J. Skaar, and V. Makarov, "Hacking commercial quantum cryptography systems by tailored bright illumination," Nature Photonics **4**(10), 686–689 (2010).
3. D. Winkler, "Practical Integration of a Quantum Channel for QKD in commercial WDM systems," M.Sc. Thesis, Vienna University of Technology, pages 95 (2013).
4. P. Eraerds, N. Walenta, M. Legre, N. Gisin, and H. Zbinden, "Quantum key distribution and 1 Gbps data encryption over a single fibr," New Journal of Physics, **12**(6), 063027 (2010).
5. K. A. Patel, J. F. Dynes, M. Lucamarini, I. Choi, A.W. Sharpe, Z. L. Yuan, R.V. Penty, and A. J. Shields, "Quantum key distribution for 10 Gb/s dense wavelength division multiplexing networks," Applied Physics Letters **104** 051123 (2014).

6. K. A. Patel, J. F. Dynes, I. Choi, A.W. Sharpe, A. R. Dixon, Z. L. Yuan, R.V. Penty, and A. J. Shields, "Coexistence of High-Bit-Rate Quantum Key Distribution and Data on Optical Fiber," Physical Review X, **2**, 041010 (2012).
7. B. Froehlich, J. F. Dynes, M. Lucamarini, A.W. Sharpe, Z. L. Yuan, and A. J. Shields, "A quantum access network," Nature **501**, 69–72 (2013).
8. I. Choi, R. J. Young, and P. D. Townsend, "Quantum information to the home," New Journal of Physics **13**, 063039 (2011).
9. L.-J. Wang, L.-K. Chen, L. Ju, M.-L. Xu, Y. Zhao, K. Chen, Z.-B. Chen, T.-Y. Chen, and J.-W. Pan, "Experimatal multiplexing of quantum key distribution with classical optical communication," Applied Phisics Letters **106** 081108 (2015).
10. T E Chapuran, P Toliver, N A Peters, J Jackel, M S Goodman, R J Runser, S R McNown, N Dallmann, R J Hughes, K P McCabe, J E Nordholt, C G Peterson, K T Tyagi, L. Mercer, and H. Dardy, "Optical networking for QKD and quantum communications," New Journal of Physics **13**, 105001 (2009).
11. A. Poppe, B. Schrenk, F. Hipp, M. Peev, S. Aleksic, G. Franzl, A. Ciurana, and V. Martin, "Integration of Quantum Key Distribution in Metropolitan Area Networks," 2014 OSA Optics & Photonics Research in Optical Sciences Congress, Quantum Information and Measurement, Berlin, Germany, 1–3 (2014).
12. S. Aleksic, D. Winkler, G. Franzl, A. Poppe, B. Schrenk, and F. Hipp, "Quantum Key Distribution over Optical Access Networks," 18th European Conference on Networks and Optical Communications (NOC 2013), pp. 11–18 (2013).
13. R. J. Runser, T. Chapuran, P. Toliver, N. A. Peters, M. S. Goodman, J. T. Kosloski, N. Nweke, S. R. McNown, R. J. Hughes, D. Rosenberg, C. G. Peterson, K. P. McCabe, J. E. Nordholt, K. Tyagi, P. A. Hiskett, and N. Dallmann, "Progress toward quantum communications networks: opportunities and challenges," Proc. SPIE 6476, Optoelectronic Integrated Circuits IX, **6476**, 6476OI (2007).
14. P. Townsend, "Simultaneous quantum cryptographic key distribution and conventional data transmission over installed fibre using wavelength-division multiplexing," Electronics Letters, **33**(3), 188–190 (1996).
15. S. Aleksic, D. Winkler, A. Poppe, G. Franzl, B. Schrenk and F. Hipp,Distribution of quantum keys in optical transparent networks: issues and challenges," 15th International Conference on Transparent Optical Networks (ICTON 2013), Cartagena, Spain, We.B1.3 (2013).
16. T. F. da Silva, G. B. Xavier, G. P. Temperão, and J. P. von der Weid, "Impact of Raman scattered noise from multiple telecom channels on fiber-optic quantum key distribution systems," Journal of Lightwave Technology, **32** (13), 2332–2339 (2014).
17. S. Aleksic, F. Hipp, D. Winkler, A. Poppe, B. Schrenk, and G. Franzl, "Impairment Evaluation toward QKD Integration in a Conventional 20-Channel Metro Network," Optical Fiber Communication Conference (OFC 2015), Los Angeles, California, USA, W4F.2 (2015).
18. S. Aleksic, D. Winkler, F. Hipp, A. Poppe, G. Franzl, and B. Schrenk, "Towards a Smooth Integration of Quantum Key Distribution in Metro Networks," 16th International Conference on Transparent Optical Networks (ICTON 2014), Graz, paper Tu.B1.1 (2014).
19. VPI Systems, *VPItransmissionMaker Optical Systems*. [Online]. Available: http://www.vpiphotonics.com/
20. D. Hollenbeck and C. D. Cantrell, "Multiple-vibrational-mode model for fiber-optic raman gain spectrum and response function," JOSA B, **19**(12), 2886–2892, (2002).
21. N. R. Newbury, "Pump-wavelength dependence of Raman gain in single-mode fibers," Journal of Lightwave Technology, **21**(12), 3364–3373 (2003).
22. R. H. Stolen, "Issues in Raman gain measurements," Tech. Dig. Symp. Optical Fiber Measurements, NIST Special Publication 953 (National Institute of Standards and Technology), Gaithersburg, MD, 139–142 (2000).

1. Introduction

Although the idea to utilize the quantum nature of optical phenomena to encrypt transmitted data is not substantially new, it was already introduced in the early 1980's [1], practical QKD systems that can be smoothly and economically integrated in conventional optical networks are still not available. Current commercially available QKD systems generally presume dedicated point-to-point fiber links connecting the two network terminals that create a common and secret key. For simplicity and in accordance with network security literature, the two terminals are called Alice and Bob. In a QKD system, quantum bits (*qubits*) are exchanged between Alice and Bob, which yields the encryption key used to secure their communication [1]. Photons received by Bob that are not originating from Alice, detected as not being in accordance to the known statistical data, indicate a potential intruder. However, if the number of noise photons exceeds a certain level, Bob is unable to detect the qubits sent by Alice, making the secure key distillation impossible. Thus, the main reason for using dark fibers to transmit qubits between Bob and

Alice is to avoid high levels of noise in the quantum channel by preventing any interaction between strong classical telecommunication channels and weak quantum channels.

On the other hand, dedicated fibers are a major drawback for an economical implementation because of the high costs of installing or leasing extra dark fibers. Additionally, QKD systems commonly require a complex on-site calibration of detectors and modulators, which are reported to be vulnerable to certain attacks [2]. Even for a system using dedicated dark fibers, achievable secret key rates are rather low (below 1 Mb/s) for distances of several tens of kilometers and above. Figure 1 presents achieved secret key rates versus link length as reported in recent experimental demonstrations and summarized in [3].

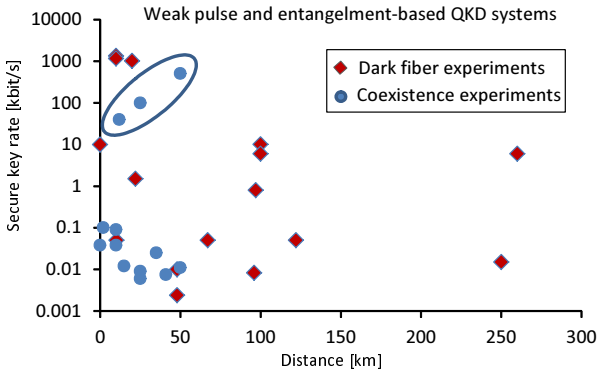

Fig. 1. QKD experiments using weak pulse and entanglement-based QKD systems.

A first step to make QKD systems more economical is to find a way to transmit weak QKD signals together with strong conventional optical signals over the same optical fiber. Such an option, referred to as *coexistence scheme*, has attracted particular interest in recent years. Several studies show that the coexistence scheme is in principle possible [4–15], but the introduced impairments strongly limit the performance of the QKD system. As can be seen from Fig. 1, the achievable secret key rate using the coexistence scheme is mostly below 1 kb/s for QKD systems based on either the weak pulse or entanglement methods, as detailed in [3]. The reported experimental results known to the authors consider systems with limited launch powers, reduced network reach and/or sparse spectral occupancy (a few active wavelength channels only). However, these restrictions on the system parameters are hardly achievable with common WDM metro network designs, in which several tens of wavelength channels and much higher power levels are used. Recently, secret key rates similar to those reported using dedicated fibers have been achieved for the coexistence scheme by optimizing the system parameters [5] (see the encircled points in Fig. 1). Key rates in the order of hundreds of kbit/s over 25 km have been demonstrated in coexistence with several classical signals at typical power levels (about 0 dBm). Moreover, the impact of Raman scattered noise from up to 14 classical channels with -10.5 dBm each has recently been studied [16]. It has been shown that an increase of the number of coexisting classical channels to more than six can severely limit both secret key rate and distance of a QKD system working at 1546.12 nm. Although a lot of effort has been put recently into investigation of the coexistence scheme, an overall characterization of possibilities and limitations upon the integration of QKD systems in conventional networks, considering typical and worst case conditions, is to the best knowledge of the current authors missing.

In this paper, we address perspectives and limitations of a smooth QKD integration in conventional metropolitan area networks and aim to find a wavelength range that best suits to allocate quantum channels. For this purpose, we analyze the impairments on quantum channels that result from many strong classical signals. The paper is structured as follows. In section 2,

we briefly outline integration options and challenges, before we examine the most dominant problem, being Raman scattering. Section 3 presents the approaches used to model and characterize Raman scattering. Section 5 introduces an experimental set-up for evaluating the QKD integration, which is based on a legacy 20-channel DWDM system. The combined experimental and simulation approach leads to the performance estimates presented in section 6. Finally, Section 7 summarizes and concludes the paper.

2. Integration of quantum key distribution in metropolitan area networks

The limited reach of weak quantum signals binds its distribution to a rather small range. To become scalable, means to cascade QKD encrypted links and to integrate QKD into conventional telecommunication networks need to be defined [18]. The scheme for a smooth integration of QKD in the metropolitan area is sketched in Fig. 2. It envisages the integration of QKD assuming the coexistence scheme, where quantum channels, the key distillation channel and all classical communication channels are transmitted over the same fiber, hop-by-hop multiplexed/demultiplexed using a so called QKD combiner/separator to sensibly add/drop/bypass the weak quantum channels.

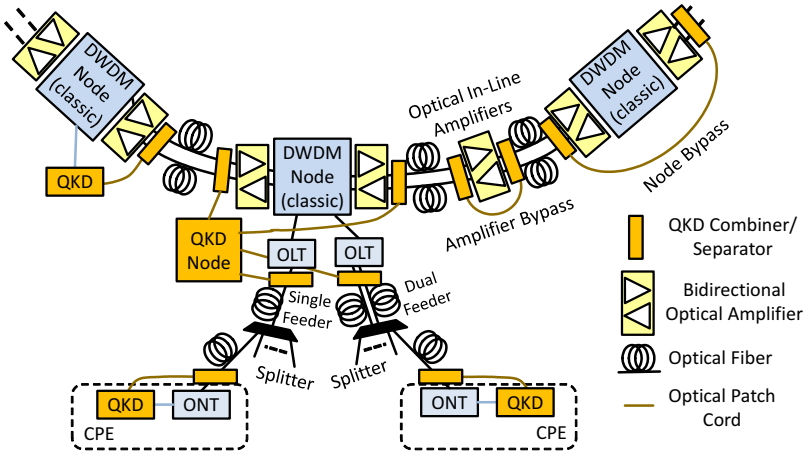

Fig. 2. Deployment of QKD in metropolitan area networks using a smooth integration in the co-existence scheme (CPE: Customer Premises Equipment, ONT: Optical Network Terminal, OLT: Optical Line Terminal).

2.1. Beyond QKD point-to-point links

To extend QKD from static point-to-point key-exchange among terminals to an end-to-end approach based on switched quantum channels, various optical components are needed: optical filters (muxes/demuxes), splitters and optically transparent switches, e.g., based on micro-electro-mechanical systems (MEMS). These components need to be specifically selected to support the weak quantum signals residing in potentially uncommon wavelength regions. Similar to the QKD combiner/separator units required to realize the co-existence approach, these are necessary to realize the transparent QKD overlay nodes.

The influence of such additional components on the quantum channel needs to be considered in the QKD overlay design because these determine the quantum signals reach, which in turn limits the span of the transparent sections and thus the QKD overlay's reach. Thus, any QKD network needs to be designed in its whole, including all signal degrading components along all

QKD paths. To share quantum channels along multiple terminal pairs, a feasible technique to multiplex/demultiplex the quantum signals is additionally required.

Topologies to be considered include point-to-point and point-to-multipoint, representing typical access topologies, as well as ring and meshed topologies, representing common metro topologies. Only put together these reveal the true topology necessary to interconnect distributed QKD terminals such that QKD enabled metropolitan area network results.

2.2. Challenges of the coexistence approach

Realizing the coexistence approach raises two specific challenges. First, quantum signals cannot pass amplifiers. These have to be bypassed using QKD combiner/separator units. Actually, if the degradation caused by any classical data network component is more than what a bypass causes, bypassing the component shall be foreseen in order to maximize the achievable secret key rate. Second, QKD systems are extremely sensitive to losses and noise. Strong conventional signals may constitute severe impairments on the weak quantum signals [6], as identified and analyzed in [11, 12, 15, 17, 18].

The 3rd transmission window around 1.5 μm (C-band), widely used for long-range communications due to the low attenuation down to 0.2 dB/km, is also very attractive for QKD systems. However, coexisting classical signals within the same band cause serious impairments [15, 18]. There have been several successful experiments demonstrating the use of the C band for QKD [5], but also showing limitations regarding the acceptable power levels and number of channels [16].

The band around 1.3 μm (O-band) shows higher attenuation of about 0.3 dB/km and is traditionally used for local area and access networks and thus today likely occupied by strong signals. Recent trends in optical access networks indicate that in order to achieve high data rates above 10 Gbit/s and due to the wide availability and maturity of the DWDM technology for the C-band, this technology will increasingly be used also in the access area within a few years' time (e.g. in NG-PON2, radio front/backhaul). Carefully taking into account all those advantages and disadvantages we decide to allocate the quantum channels in the 1.3 μm region (O-band) under assumption that conventional channels will reside in the C-band. As a consequence, the influence of numerous nonlinear effects such as four-wave mixing, Brillouin and Rayleigh scattering can be avoided by allocating the quantum channel spectrally far away from classical data channels. However, Raman scattering still represents a source of bothersome noise photons in the quantum channel, even if the spectral separation between the quantum and classical channels is 200 nm and more, as here assumed.

3. Modeling of Raman scattering

Scattering effects in the fiber medium poses one of the major sources of the noise in QKD channels. The scattering related to acoustic vibrations (Brillouin scattering) can be mostly neglected because of its low bandwidth (1-10 GHz), so Brillouin scattering does not have a considerable influence on QKD channels positioned spectrally far away from classical channels. In contrast, Raman scattering, where optical phonons are involved, introduces large spectral shifts with a large offset from the incident (pump) wavelength. In case of Stokes scattering, part of the photons energy is absorbed by the fiber resulting in the generation of scattered waves at lower frequencies. On the other hand, the resulting excited phonon energy is transferred to a photon at a higher frequency, i.e., a lower wavelength, in an anti-Stokes process. The anti-Stokes scattering is less effective as it requires the pre-existence of vibrational modes, which makes the wavelengths below the wavelength of data channels more preferable for QKD. While this difference is not significant for fibers at room temperature, an allocation of QKD channels below the wavelength of crosstalk-inducing data channels, e.g. in the O-band, offers additional

benefits such as using the standard telecom components for the O-band and enjoying a large spectral separation from the C-band wavelengths.

For optical fibers, the Raman gain is usually defined by the Raman gain coefficient, $RGC(f_p, \Delta f)$ [m/W]. This gain relates the power of the pump, f_p, and the scattering strength (offset by Δf) and can be experimentally measured. For modeling purposes, the Raman gain can be characterized by the Raman gain factor, $g(f_p, \Delta f)$ [$\frac{1}{Wm}$], which is the Raman gain coefficient divided by the effective core area of the fiber, A_{eff} [m^2]. Raman gain profiles containing the chosen pump frequency, f_p, and the measured Raman gain factor across a frequency offset range, Δf, can be used in simulations in order to roughly evaluate the noise magnitude in the quantum channel. This profile is independent of fiber dimensions such as A_{eff} and can be re-scaled on-the-fly according to chosen pump wavelengths and signal powers.

A fiber model based on a solution of the full Schrödinger equations as implemented in the commercial simulation tool *VPITransmissionMaker* [19] is used for simulation studies. The Raman gain profiles are adapted to fit our measurements. The original maximum offset parameter has been extended from 35 THz to more than 50 THz and a new Raman gain profile generated by implementing the intermediate-broadening model [20] and using data obtained by measurements. The intermediate-broadening model provides a simple analytic expression which fits the shape of the Raman gain spectrum and the Raman response function of silica fibers. The approach utilizes a convolution of Lorentzian and Gaussian functions that represent multiple vibrational modes. For example, the sharp peak in the Raman spectrum of silica fibers at around 400 cm^{-1} offset corresponds to the bending of an Si-O-Si dihedral angle. At this offset each Lorentzian peak can be seen as a physical representation of a different equilibrium value of the dihedral angle [20]. The expression for the Raman response functions is

$$h_R(t) = \sum_{i=1}^{13} \frac{A_i^{'}}{\omega_{\upsilon,i}} exp(-\gamma_i t) exp(-\Gamma_i^2 t^2/4) sin(\omega_{\upsilon,i}) \theta(t) \tag{1}$$

and the Raman gain function (i.e., the Fourier transform of the Raman response functions) is given by

$$s(\omega) = \sum_{l=1}^{13} \frac{A_i^{'}}{2\omega_{\upsilon,i}} \int_0^{\infty} exp(-\gamma_i t)\, exp(-\Gamma_i^2 t^2/4) \{cos[(\omega_{\upsilon,i} - \omega)t] - cos[(\omega_{\upsilon,i} + \omega)t]\}\, \mathrm{d}t, \tag{2}$$

where $A_i^{'}$ is the amplitude of the i^{th} vibrational mode, $\omega_{\upsilon,i}$ is the center vibrational frequency for mode i, γ_i and Γ_i are Lorentzian and Gaussian mode linewidths, respectively. $\theta(t)$ represents the unit step function, being one for $t \geq 0$ and zero otherwise. Note that we use here, similar to the approach presented in [20], thirteen Gaussians with various widths and amplitudes that are centered at various frequency offsets, where each Gaussian corresponds to a different vibrational mode in fused silica.

The envelope curve generated from Eq. 2 is only proportional to the Raman gain spectrum and needs to be normalized. The peak of the envelope curve has to be chosen as reference point and the scaling performed according to the peak amplitude of the SMF-28 NIST reference curve [21,22] and other empirical data. The resulting Raman gain spectrum is depicted in Fig. 3. We performed measurements to verify our simulation model. Both simulation and measurement are shown in the inset of Fig. 4.

4. Simplified model of a QKD system

The selection of an appropriate wavelength for a QKD link as discussed in Section 2.2 is based on assumptions regarding its resistance against uncorrelated noise photons. Highly optimized

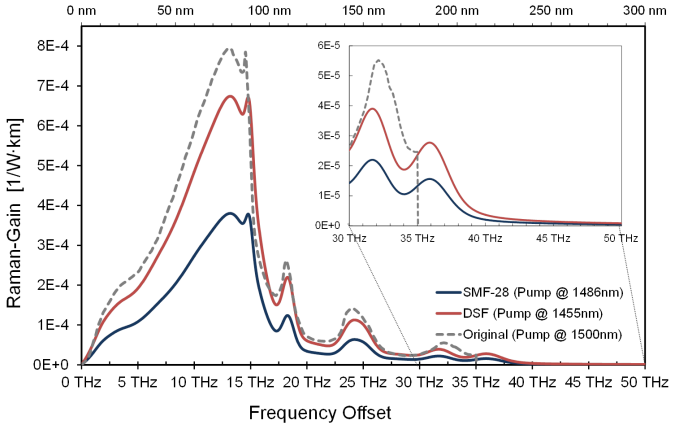

Fig. 3. Raman gain profile as used in simulations.

systems [6] with narrow-band attenuated laser emission and accurate filtering in wavelength and time can extract the photons carrying modulated qubit information much better than typical university research systems designed for operation at dark fibers. In the case these research systems are embedded in telecom equipment, they will suffer from background noise generated by telecom communication carriers. This work indicates the level of expected background photons to select the right wavelength regime for the quantum channel. With the following simplified model of a QKD system we introduce an indicative acceptance rate of 1 million noise photons per second and nanometer for a reliable operation [15].

For Alice we assume a weak laser pulse system operated at a pulse repetition rate of 10 MHz (limited by the detector opening frequency) and a typical number of photons/pulse of $\mu = 1/10$. The quantum channel is ideal, but suffers from transmission losses. We assume here a transmission loss of 13 dB. At the receiver, Bob can expect the arrival of approximately 50,000 photons per second. InGaAs SPADs are gated with 10 MHz in accordance to the expected photon rate with a time window of 1ns, so photons are detected only during a time period of 10 ms within a second. For the sake of simplicity, we do not consider here the effect of the detector dead time. Assuming the use of the BB84 protocol, every in-band noise photon reaching the detectors within this 1% of time in which detection is possible has the chance of 50% to cause an error event. To the end, overall 100,000 background photons per second would generate an additional quantum bit-error rate (QBER) of 1%. A filtering in wavelength by commercial 25 GHz-DWDM grid filters would reduce the noise photon flux and allow $\approx 10^6$ photons/(s·nm) to cause an additional QBER in the order of few percent. We will use this value in the following diagrams as a guide to the eye.

5. Combined QKD and metro networks

To enable a reliable exchange of qubits in presence of strong classical signals an accurate consideration of the impairments caused by Raman scattering and an effective noise filtering in the O-band are essential. We first concentrate on defining and analyzing the method for combining and separating QKD and classical signals by spectral filtering. A cascade of two band multiplexers/demultiplexers (far wavelength-division multiplexers - FWDMs) is used as shown in Fig. 4, because with a single typical band filter sufficient band rejection cannot be achieved. Additionally, a narrow-band filter (0.1 nm) is needed in front of the QKD receiver to further reduce the noise level. The experimental setup depicted in Fig. 4 is applied to experimentally analyze the combining/separating of quantum and classical channels and also to evaluate the

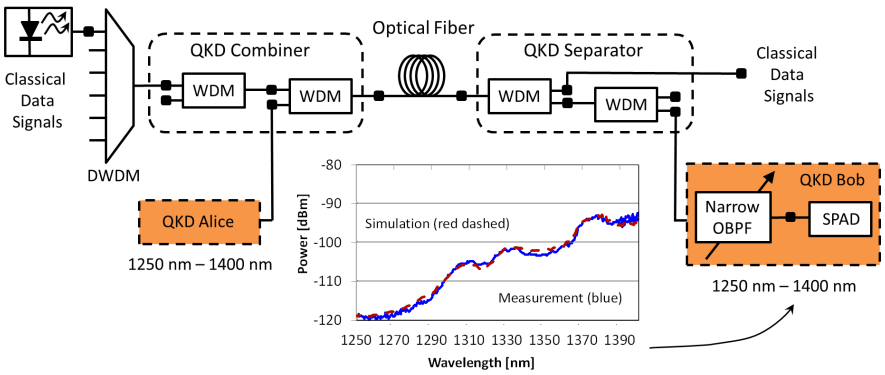

Fig. 4. Experimental and simulation setup for analyzing the influence of forward Raman scattering on integrated QKD systems in metropolitan area networks. Inset measurement and simulation results for 14 km of standard single mode fiber (SSMF) and the wavelength range from 1250 nm to 1400 nm. The resolution bandwidth was 0.1 nm in both cases (measurement and simulation). FWDM: Far Wavelength Division Multiplexer.

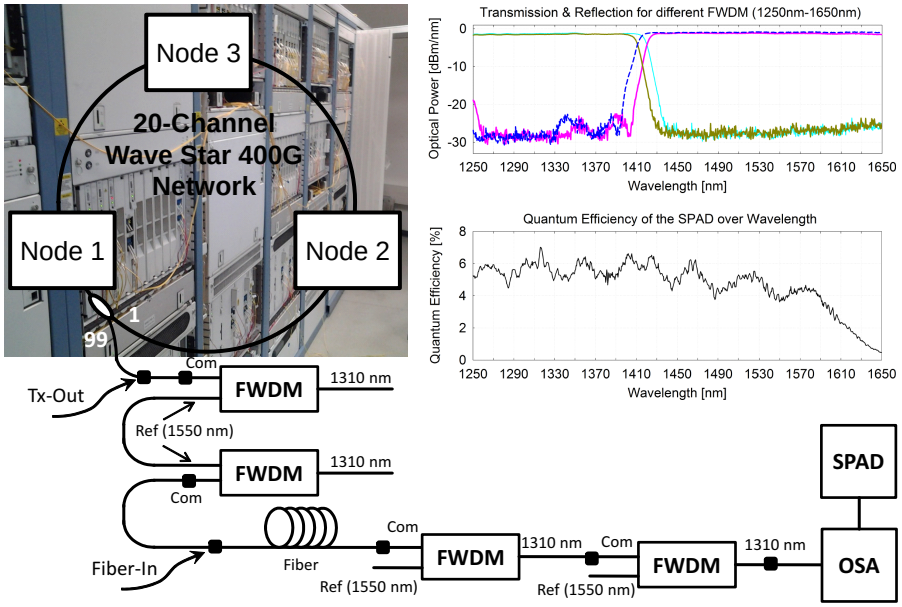

Fig. 5. Experimental setup for characterization of QKD integration in metropolitan area networks. Inset measured transmission and reflection curves for different FWDM components used to combine/separate quantum and classical channels as well as measured quantum efficiency of the single photon avalanche photodiode (SPAD) used to count noise photons below 1410 nm.

influence of Raman scattering. Because noise levels below -90 dBm can hardly be measured with conventional optical spectrum analyzers (OSA), we count the noise photons using a single-photon avalanche photo diode (SPAD). A narrow coherent 1550.12 nm continuous-wave (CW) laser source with 3.5 dBm optical output power is used as Raman pump. The measured forward Raman scattering in a 14 km long standard single mode fiber (SSMF) is shown inset in Fig. 4 together with the simulation result (dashed lines). At 1250 nm the noise level is as low as -120 dBm and increases toward longer wavelengths. Above 1360 nm and 1400 nm the optical

noise power rises above -100 dBm and -95 dBm, respectively, which already prohibits reliable exchange of qubits in these spectral regions. Experimental and simulation results fit very well over the wavelength range of interest, i.e., between 1250 nm and 1400 nm.

6. Characterization of QKD integration

We analyze the performance of QKD integration in the metropolitan area by applying a combined experimental and simulation approach. First, we configured a 3-node commercial DWDM system (Lucent Wave Star OLS400G) to provide 20 DWDM channels (classical data channels). A generic picture of the configured ring network containing 3 nodes is shown in Fig. 5. The 20-channel DWDM signal generated in node 1 and amplified by a booster erbium-doped fiber amplifier (EDFA) is tapped off using a 99/1 optical coupler. Cascaded 1310/1550 far wavelength-division multiplexers (FWDMs) are used for combining and separating quantum channels with classical data channels and to further suppress the background noise in the O-band to a tolerable level. Measured transmission and reflection curves for FWDM components and quantum efficiency of the SPAD are shown inset. Note that the SPAD is used to count noise photons within the O-band, while the spectrum above 1410 nm is measured using an OSA.

6.1. QKD link

In order to reflect the variety of installed fiber types, we choose standard (ITU-T G652-B) and low-water-peak single mode fibers (G652.D) of different age and length. Additionally, to address the influence of connectors and splices, we consider a 27 km long fiber made of two pieces (14 km and 13 km) that are connected with each other by connectors. The fibers are characterized by a white light source to obtain the attenuation curve. The measurement results are presented in Fig. 6.

We performed measurements on the fibers characterized in Fig. 6 using the setup shown in Fig. 5. As can be seen from Fig. 7, the noise within the O-band is mainly caused by the forward Raman scattering. A noise level below 1 million photons/(s·nm) has been obtained up to 1310 nm, for all fiber types and lengths considered. The difference in noise levels between the considered fibers lies within a range of 10 dB. This emphasizes the need for characterization of the installed fibers prior to considering QKD integration. Coexisting strong signals within the C-band, i.e., the 20-channel DWDM signal, the optical supervisory channel (OSC) at 1510 nm and the residual power of the filtered EDFA pump at about 1480 nm, cause a reduction of the useable wavelength range for about 60 nm when comparing to the single channel measurement shown in Fig. 4.

Since scattered signals propagate in both forward (together with data signals) and backward (in opposite to data signals) directions, we also have to consider the backward Raman. In systems where either telecom or quantum signals are transmitted bidirectionally, which can be the case in some access networks, the backward Raman scattering becomes important. In order to measure the effect of backward Raman scattering, we slightly modify the experimental setup presented in Fig. 5 by connecting the fiber input to the common (Com) output of the third FWDM device (see Fig. 8). Thus, the DWDM signal enters the fiber through the Com port, while the backward scattered (as well as reflected) photons pass through the reflective (Ref) port to be further filtered by the fourth FWDM and counted by SPAD and OSA.

The noise spectrum measured using the setup depicted in Fig. 8 is shown in Fig. 9. The obtained available wavelength range is similar to that obtained for the forward scattering. However, the difference in noise levels for long and short fibers is lower. Moreover, the effect of Raman backward scattering is strongest for the 14 km long fiber, which is an expected outcome. This is due to a higher attenuation in longer fibers, which effects both pump signal and

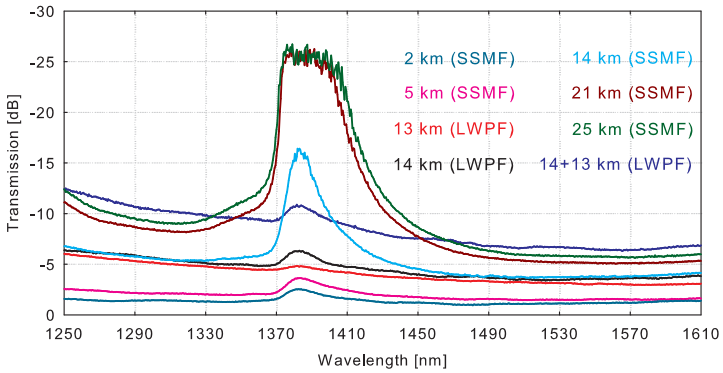

Fig. 6. Characterization of fiber attenuation for different fiber types and lengths obtained using a white light source. Low-water-peak fibers (LWPF) and standard single mode fibers (SSMF) in one piece or made from two pieces (14 km + 13 km) are chosen to reflect the variety of installed fibers.

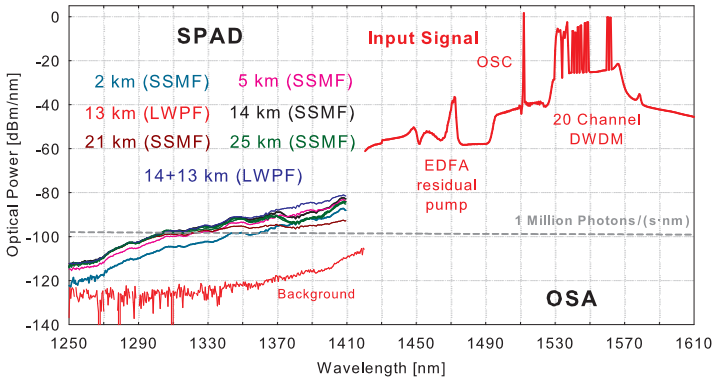

Fig. 7. Forward Raman scattering: noise power level within the O-band caused by the strong classical signals in the C-band of a conventional DWDM system in operation. Results are shown for different fiber types and lengths. Also background noise of the signal before transmission is shown (red line).

scattered photons. Since the pump power decays exponentially with fiber length, the major contribution of noise is saturated at a certain fiber length and gets reduced by exceeding this threshold.

In order to estimate the contributions of the data channels, the optical supervisory channel (OSC) and the residual EDFA pump to the noise in the O-band, we carried out measurements with OSC only, with OSC and EDFA pump and with OSC and data channels without EDFA pump. The input signals used to characterize the main cause of the noise are obtained by using appropriate filters to split up the signal generated by node 1 into signals I to IV presented in Fig. 10.

The corresponding results for cases I to IV and a fiber length of 14 km are shown in Fig. 11. The blue curve represents the measured photon noise level in the O-band when the DWDM signal and the residual EDFA pump are removed (case II). Here, the background noise noise is only due to the OSC signal. Even though OSC is only a single channel, it has a significant influence on the noise generated in the O-band since it is allocated at least 20 nm closer to the quantum channel than the data channels. To obtain the green curve representing case IV, we filter out the DWDM signal. Here, an increase of the photon noise by about 2 dB in comparison

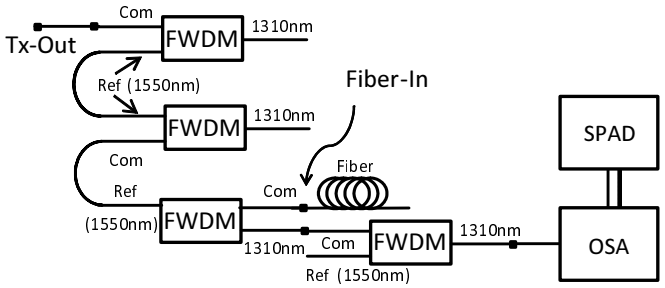

Fig. 8. Setup for measuring the noise level caused by backward Raman scattering.

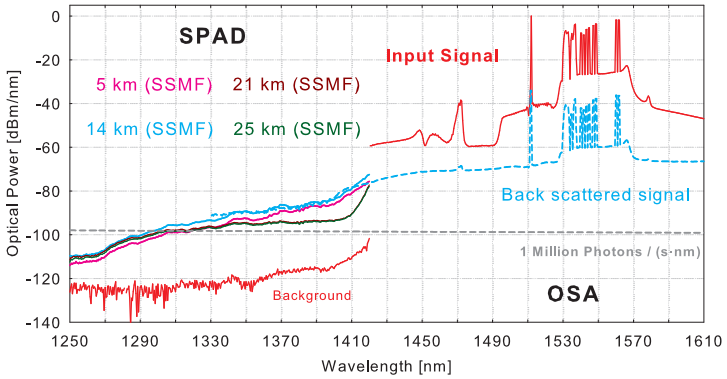

Fig. 9. Backward Raman scattering: noise power level within the O-band caused by the strong classical signals in the C-band of a conventional DWDM system in operation. Results are shown for different fiber types and lengths. Also background noise of the signal before transmission is shown (red line).

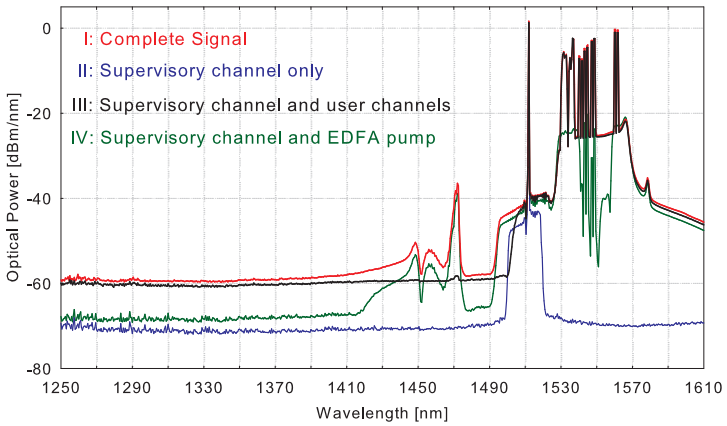

Fig. 10. Fiber input signals for characterizing the main cause of the Raman-generated noise in the O-band measured by an OSA.

to case II has been observed, which is mainly due to the EDFA's amplified spontaneous emission (ASE) noise. Finally, we filter out the residual EDFA pump only in order to assess its influence. The corresponding noise spectrum is shown by the black curve (case III), which is almost identical to the red curve (case I - entire signal) for the forward and lies slightly below it for the backward scattering. This result indicates that the influence of the residual EDFA pump

signal can be neglected. Even though it is spectrally closer to the O-Band than the OSC, its low power (about -40 dBm) does not suffice to generate many scattered photons in the O-band. The 20-channel DWDM signal contributes by up to 5 dB to the photon noise. This significant contribution varies with wavelength, the number of classical channels and their power levels.

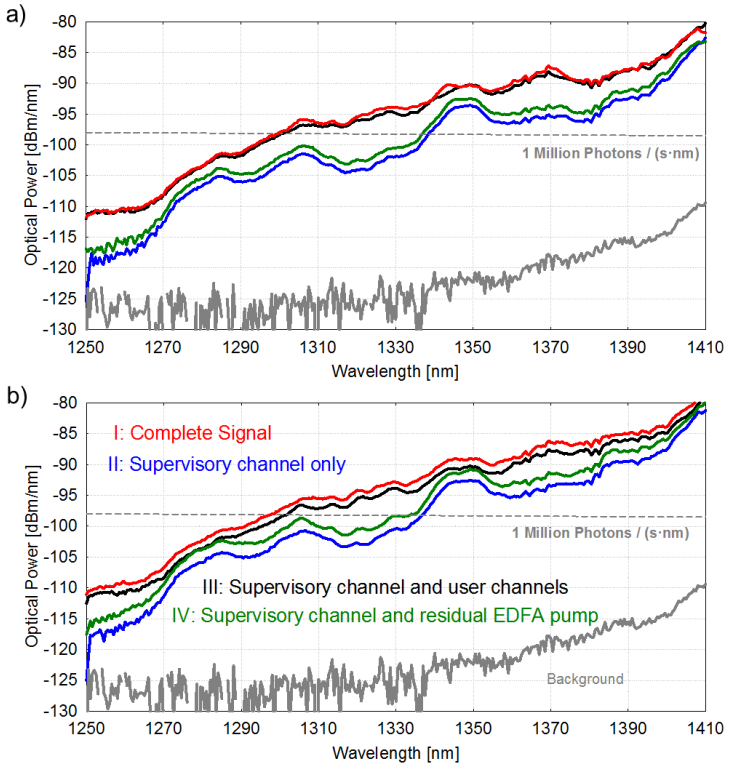

Fig. 11. Contributions of signals I, II, III and IV (see Fig. 10) to the noise in the O-band a) for forward and b) backward scattering. Also background noise of the signal (back-to-back) before transmission is shown (grey line).

6.2. Add/Drop filters for implementing QKD combiners/separators

The presented experimental results are obtained using FWDM filters that separate incoming and outgoing wavelengths above and below about 1420 nm, as it is shown in the inset of Fig. 5. By introducing FWDM filters with a separation at 1510 nm a fifth input signal can be generated, which comprises the DWDM classical data signals only, while the supervisory channel and EDFA residual pump are suppressed. In analogy to the setup shown in Fig. 4, two cascaded 1510 nm-FWDM filters are inserted before the fiber input. The supervisory channels' power is hereby attenuated by about 35 dB and the residual EDFA pump is completely suppressed. The input is displayed by the dashed brown line in Fig. 12.

In order to separate the outgoing C- and O-band signals after the fiber, two FWDMs are once again needed. As it turns out a cascade of 1520 nm FWDM filters is not sufficient to suppress the background noise below -100 dBm and is therefore unsuitable to distinguish the originated impairments at such low energy levels. We therefore employ the well tried 1410 nm FWDMs after the fiber for our experimental setup. The Raman curve resulting from this combination of 1510 nm filters before and 1420 nm FWDMs after the investigated 14 km fibre is shown by the brown line in Fig. 12 (Input V). The comparison with the results obtained using the

inputs II and III (Fig. 10), where the supervisory channel is fully present, is shown in Fig. 13. As indicated by the black arrows, the generated noise spectra shows an inverted behavior for certain wavelengths depending on whether the OSC is fully present or not. This behavior can be explained as follows. Depending on the wavelength and the strength of classical signals certain modes seem to become more or less dominant, which causes a wavelength dependence of the Raman counts with respect to input signal wavelengths. This is particularly interesting for the wavelength window between 1310 nm to 1350 nm. Here, the absence of the data signals causes a drop in counts of almost 10 dB.

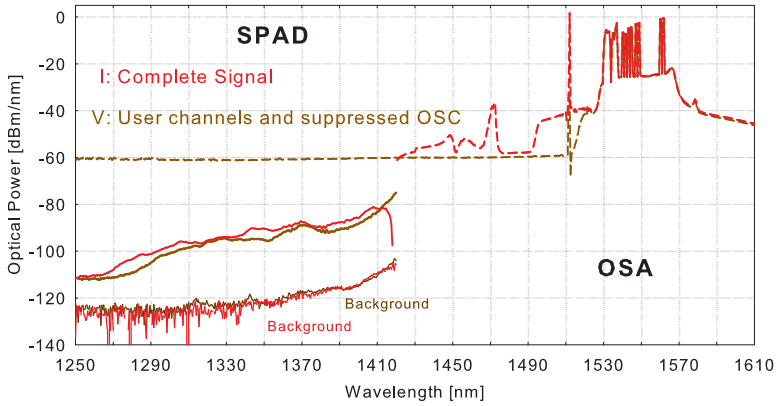

Fig. 12. Raman counts obtained for 14 km SSMF using 1510 nm and 1410 nm FWDM.

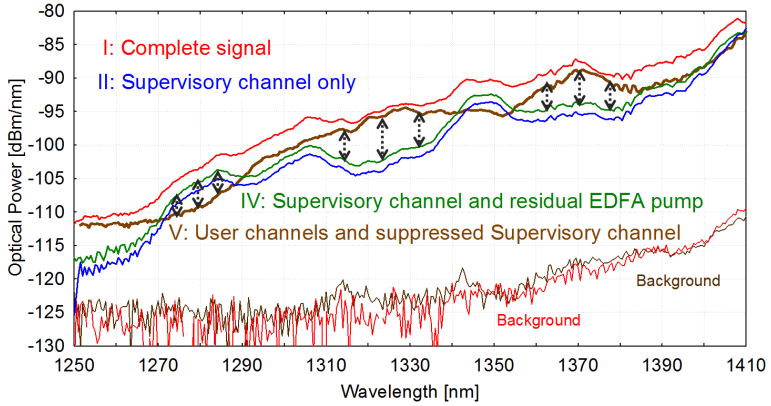

Fig. 13. Raman scattering caused by signals with optical supervisory channel (OSC) (II and III) show a different behavior from the signal with suppressed OSC.

6.3. QKD bypass

As already mentioned in Section 2, a smooth integration of QKD able to provide an end-to-end data encryption in the metropolitan area presumes implementing methods for multiplexing and switching of quantum channels as well as an efficient bypass of some conventional network elements. Since weak quantum signals cannot pass opaque network nodes and amplifiers without being destroyed, those elements have to be bypassed. An efficient bypass of amplifiers and network nodes can be realized using two QKD combiners/separators and a short piece of fiber to directly connect them, thereby providing a low-attenuation bypass for quantum channels,

while data channels are being processed as usual. The simulation setup we use to analyze the influence of the amplifier and node bypass is is shown in Fig. 14 a) and Fig. 14 b), respectively. Similar to the experimental setup shown in Fig. 5, we generate a 20-channel DWDM signal together with an OSC signal at 1510 nm. The signal generated in the simulator and launched into the fiber perfectly mimics the measured signal shown in Fig. 10 - case I (complete signal). We set all the simulation parameters such as fiber characteristics, background noise spectrum and power/bandwidth of all signals according to the measured data.

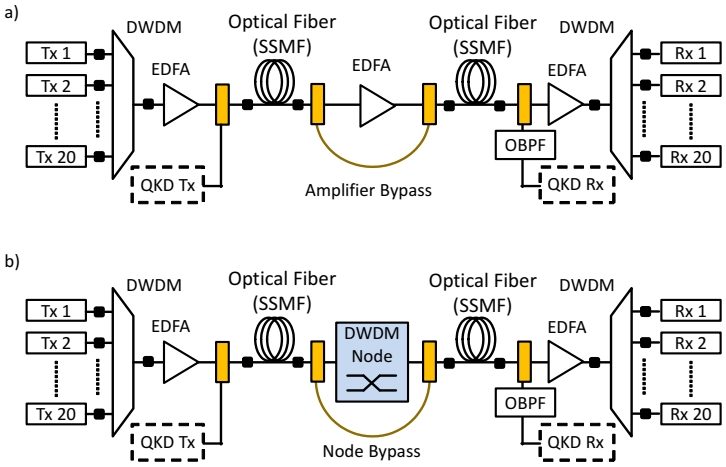

Fig. 14. Simulation setup for characterizing a) amplifier bypass and b) node bypass. Note that the bypassed node is assumed to be opaque, i.e., the incoming DWDM signal is terminated at the input and a new one generated at the output. EDFA: Erbium-Doped Fiber Amplifier.

The simulation results for amplifier and node bypass are presented in Fig. 15. For comparison purposes, we also show the spectrum of the 14-km point-to-point link (red curve in Fig. 15). It is evident that the additional filtering needed for bypass causes a reduction of the noise in the O-band, also through suppressing the noise generated within the C-band in the first fiber span, which has a positive impact on the Raman noise being generated within the O-band in the second span. Especially the bypass of an opaque node, as depicted in Fig. 14 b), benefits from a noise reduction of more than 10 dB in comparison to the line without bypass because the signal from the first span is terminated in the node and a new, low-noise one generated. As regards fiber length, the minimum noise level is obtained, as expected, for 2×2.5 km, while for 2×10 km, the generated noise is highest. This is in agreement with the experimental results reported in Figs. 7 and 9 because similar reasoning regarding attenuation of Raman noise in longer fibers also holds here.

As already mentioned, weak quantum signals are not only affected by noise photons, but also are significantly impaired by attenuation. The two QKD combiners/separators required for QKD bypass introduce about 1 dB of attenuation each, which causes about 2 dB additional loss in the bypass configuration. However, for typical distances in the metropolitan area, the attenuation of optical fibers contributes considerably more to the overall loss than the QKD combiners/separators. For example, attenuation introduced by 40 km of SSMF is about 12 dB for the O-band, which is six times higher than the insertion loss of a QKD combiner/separator. On the other hand, the impact of the increased loss of QKD bypass is compensated by the reduced noise level (see Fig. 15).

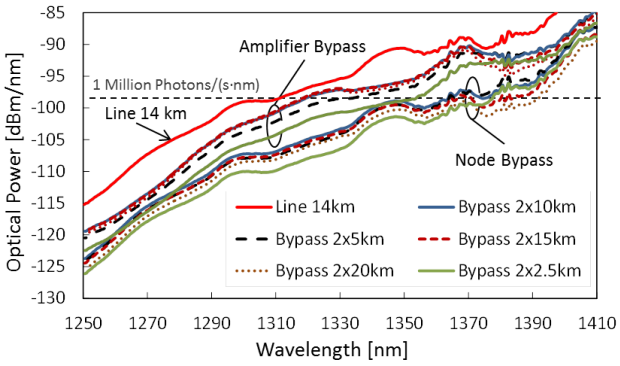

Fig. 15. Simulation results for amplifier and node bypass.

6.4. Discussion

As the presented measurements show, an integration of QKD systems into existing metro and access networks boils down to the question whether a QKD scheme can be found that withstands the high noise levels almost entirely caused by Raman scattering originating from the multiplexed strong classical data channels. Although an elaborated positioning of classical channels and quantum channels may reduce noise to a tolerable level for the quantum channel, key rate and user scaling still remain challenging issues. Possible approaches to tackle these problems are filtering in the time and the wavelength domain. The latter can be achieved with standard equipment used in telecommunication networks, as shown in the presented approach that propose the allocation of quantum channels in the O-band. For wavelengths shorter than 1310 nm the noise can be reduced to acceptable levels. This approach allows bypassing active network components such as optical nodes and amplifiers as well as potential multiplexing and switching of quantum signals towards QKD networks. However, without appropriate time filtering the photons of interest are hard to separate from noise. Recently developed detectors with gating times in the sub-ns range are able to reduce noise by about 10 dB [6], making it likely to detect a photon sent by Alice, when exact timing information is available.

7. Conclusions

In this paper, we proposed and investigated an approach for reliable exchange of quantum keys over existing fiber infrastructures in coexistence with many classical (conventional) data channels operated at usual power levels. In particular, we analyzed the influence of Raman scattering caused by a commercial 20-channel DWDM system on quantum channels allocated in the O-band (around 1.3 μm). The presented measurements show that an elaborated positioning of classical and quantum channels and filtering in the time and wavelength domains can reduce the noise to a tolerable level for a QKD system. The positioning of quantum channels in the O-band simplifies the bypassing of active network equipment such as network nodes and amplifiers as well as multiplexing and switching of quantum signals toward QKD networks. This approach enables the use of standard equipment to realize a smooth integration of quantum key distribution (QKD) systems in deployed metropolitan area networks.

Acknowledgment

This work has been supported in part by the project ”QKD-Telco: Practical Quantum Key Distribution over Telecom Infrastructures” (contract No. 835926), within the FIT-IT programme funded by the Austrian Federal Ministry for Transport, Innovation and Technology (BMVIT) in coordination with the Austrian Research Promotion Agency (FFG).